Published in final edited form as:
AJR Am J Roentgenol. 2009 December ; 193(6): 1500–1503. doi:10.2214/AJR.09.3365.

Imaging Findings in a Fatal Case of Pandemic Swine-Origin Influenza A (H1N1)

Daniel J. Mollura[1], **Deborah S. Asnis**[2,3], **Robert S. Crupi**[4], **Rick Conetta**[5], **David S. Feigin**[6], **Mike Bray**[7], **Jeffery K. Taubenberger**[8], and **David A. Bluemke**[1,6]

[1]Department of Radiology and Imaging Sciences, National Institutes of Health, Clinical Center, Bethesda, MD

[2]Department of Infectious Diseases, Flushing Hospital Medical Center, Flushing, NY

[3]Department of Medicine, Weill Cornell Medical College, New York, NY

[4]Department of Emergency Medicine, Flushing Hospital Medical Center, Flushing, NY

[5]Department of Critical Care Medicine, Flushing Hospital Medical Center, Flushing, NY

[6]Russell H. Morgan Department of Radiology and Radiological Science, Johns Hopkins University, 600 N Wolfe St., Baltimore, MD 21287

[7]Integrated Research Facility, National Institute of Allergy and Infectious Diseases, National Institutes of Health, Bethesda, MD

[8]Viral Pathogenesis and Evolution Section, Laboratory of Infectious Diseases, National Institute of Allergy and Infectious Diseases, National Institutes of Health, Bethesda, MD

Abstract

Objective—Although most cases of swine-origin influenza A (H1N1) virus (S-OIV) have been self-limited, fatal cases raise questions about virulence and radiology's role in early detection. We describe the radiographic and CT findings in a fatal S-OIV infection.

Conclusion—Radiography showed peripheral lung opacities. CT revealed peripheral ground-glass opacities suggesting peribronchial injury. These imaging findings raised suspicion of S-OIV despite negative H1N1 influenza rapid antigen test results from two nasopharyngeal swabs; subsequently, those results were proven to be false-negatives by reverse transcriptase polymerase chain reaction. This case suggests a role for CT in the early recognition of severe S-OIV.

Keywords

chest CT; emergency medicine; H1N1; infectious diseases; multifocal ground-glass opacities; swine-origin influenza A

The appearance in March 2009 of a novel swine-origin influenza A (H1N1) virus (S-OIV) as a cause of human disease in Mexico and its rapid spread throughout the world marked the beginning of the first influenza pandemic in more than 40 years [1,2]. Concern for the potentially devastating impact of a novel influenza virus, to which the entire global population lacks immunity, has been heightened by awareness of the high case fatality rate seen in the 1918 influenza pandemic and in recent cases of highly pathogenic H5N1 avian influenza [3, 4]. Epidemiologic data to date suggest that the newly emerged H1N1 virus, although

Address correspondence to D. A. Bluemke (David.Bluemke@nih.gov).

transmissible from person to person, is of relatively low virulence [5]. However, as in the case of seasonal influenza, even an agent with low pathogenicity for healthy children and adults can still cause lethal disease in young infants, pregnant women, elderly individuals, and persons with immune deficiency or other chronic medical conditions. It is therefore essential that clinicians be able to recognize possible cases of pandemic H1N1 influenza in high-risk groups so that they order the appropriate diagnostic tests, begin specific antiviral therapy, and prepare to provide intensive supportive measures as needed. The role of radiologic imaging in epidemic detection and response is evolving, with imaging being used as a tool for identifying severe cases [6,7]. In this article, we describe the radiologic appearance of a fatal case of novel swine-origin influenza A (H1N1) virus (S-OIV).

Case History and Radiology Findings

A middle-aged man with no history of chronic pulmonary disease presented to the emergency department with a 5-day history of fever, fatigue, nausea, and diarrhea. He complained of an intermittent cough for approximately 3 days and confusion the night before presenting to the hospital. He denied smoking and recreational drug use. Admission vital signs included a fever of 103.3°F, blood pressure of 92/53 mm Hg (systolic/diastolic), pulse of 84 beats per minute, respiration of 22 breaths per minute, and oxygen saturation of 95% on bilevel positive airway pressure (BiPAP) ventilatory support. Physical examination was notable for a confused mental status, bibasilar pulmonary crackles on auscultation, and obesity. WBC count was 10,600 cells/mm^3. Serum chemistry results were notable for an elevated creatinine level of 3.2 mg/dL. Head CT depicted normal findings. Because of the patient's confusion and lethargy, lumbar puncture was performed and showed unremarkable serologies. The initial nasopharyngeal swab for H1N1 influenza rapid antigen test was performed twice, yielding negative results.

A portable bedside chest radiograph obtained at the initial evaluation (Fig. 1A) showed peripheral patchy opacities. Hilar fullness, possibly accentuated by hypoinflation of the lungs, was noted. The patient continued to have severe hypoxia despite BiPAP ventilation and was intubated later that day. The patient was started empirically on IV antibiotics, oseltamivir, and corticosteroids.

Chest CT (Figs. 1B–1E) was performed on day 1 of admission and showed a peripheral distribution of patchy ground-glass opacities. Many of the opacities showed air bronchograms with normal-sized bronchial airways leading into each rounded ground-glass focus, and most large airways showed no significant wall thickening or plugging (Fig. 1F). The ground-glass opacities were located throughout the upper and lower regions of all lobes in a peribronchovascular distribution. CT showed no evidence of a mosaic perfusion pattern, suggesting no localized air trapping or regional changes in blood flow. There was an absence of centrolobular nodularity or tree-in-bud opacities, suggesting the absence of small-airway inflammation in the secondary lobules. IV contrast material could not be administered to the patient because of progressing renal failure.

Chest CT in soft-tissue windows (not shown) displayed several notable negatives including the absence of mediastinal lymphadenopathy as well as the absence of pleural or pericardial effusions. Echocardiography (not shown) revealed moderate concentric left ventricular hypertrophy and an ejection fraction of 58% with mild-to-moderate tricuspid regurgitation. A more sensitive reverse transcriptase polymerase chain reaction (RT-PCR) test of a nasopharyngeal swab was reported positive on day 2 for H1N1 swine-origin influenza A virus, thereby reversing the original less sensitive negative rapid influenza test results [8]. Urine was negative for pneumococcal and *Legionella* antigens. Cultures of blood, urine, CSF, and sputum were negative for abnormal flora.

With institutional review board approval, parenteral ribavirin was initiated 40 hours after presentation in addition to the oseltamivir that had been started on day 1. Hypoxia, renal failure, and acidosis continued to progress, and the patient died on the fifth hospital day. Because of the severity of the patient's illness, repeat CT was not performed and bedside portable radiography was limited.

A postmortem examination was performed, and gross pathologic examination of the lungs revealed patchy regions of parenchymal discoloration in all lobes bilaterally, in agreement with the CT and radiographic evidence of multiple patchy air-space ground-glass opacities. Gross pathology showed no evidence of pulmonary emboli or infarction. Histologic examination of the lungs showed areas of intraalveolar hemorrhage with fibrinous material, proteinaceous fluid, macrophages, and reactive pneumocytes in addition to RT-PCR and immunohistochemical confirmation of novel H1N1 infection. These pathologic findings are consistent with a primary influenza viral pneumonitis leading to diffuse alveolar damage and acute respiratory distress syndrome (ARDS) clinically [9] and correspond to the described imaging features showing severe injury to peribronchial spaces. Other findings noted at autopsy were stenoses of the left anterior descending and lateral circumflex coronary arteries, both of which were approximately 75% occluded, and evidence of an old subendocardial anterior wall infarct, but no evidence of acute myocardial ischemia or coronary thrombus.

Discussion

CT findings on the day of hospital admission revealed peripheral distribution of segmental and subsegmental patchy peribronchovascular ground-glass opacities throughout all regions of the bilateral lungs. Characterization as ground-glass opacities is supported by the observation that the underlying lung architecture was discernible for most of these foci. Ground-glass opacities are generally pathologically attributable to the partial displacement of air from partial filling of air spaces, thickening of interstitial tissues from fluid or cells, partial alveolar collapse, or increased capillary blood volume [10–12]. The imaging findings in this case, therefore, suggest a differential diagnosis of atypical infection (including viral infection; *Mycoplasma*, *Chlamydia*, or *Legionella* infection; and septic emboli), ARDS, cryptogenic organizing pneumonia (COP), eosinophilic pneumonitis, and hypersensitivity pneumonitis [13,14].

The observed pattern in our patient differs from hydrostatic or cardiogenic pulmonary edema, which usually shows a perihilar distribution of confluent ground-glass opacity and associated pleural effusions [13,14]. A striking feature of this case is the predominance of rounded multifocal ground-glass opacities in peribronchovascular distribution. Figure 1F shows a magnified view of this finding in which the airway is less radiographically involved and the ground-glass opacification of the surrounding peribronchial structures is evident. The absence of a mosaic perfusion pattern weighs against small-airway obstruction with air trapping and regional blood flow abnormalities, which have otherwise been described in viral pneumonias [13–16]. The absence of centrolobular and tree-in-bud opacities further decreases the suggestion of bronchiolitis and small-airway inflammation at the level of the secondary lobule.

The medical literature contains few presentations of radiologic findings in seasonal influenza probably because of the nonspecificity of and frequently confounding features from coinfection and multifactorial lung injury, with most cases not being sufficiently severe to warrant imaging. Historically, seasonal influenza has been associated with heightened mortality due to superinfection from community-acquired pneumonias in which the radiographic pattern may be lobar and nonsegmental [16–19] in contrast to the multifocal patchy peripheral distribution seen here. Additionally, comorbidities have added to this mortality and complicated the imaging findings [20–22].

In a recently published series of 18 cases of fatal S-OIV infection in Mexico [2], investigators reported that patchy bilateral opacities were seen on radiography in all patients and that one CT image showed ground-glass air-space density. Although that report provided a limited description of the radiologic features, our findings are consistent with and add detail to the characterization of lung injury resulting from H1N1. Radiographic abnormalities in some recent cases of H5N1 avian influenza showed that consolidations were segmental and lobar, sometimes in a bilateral perihilar distribution or a unilateral segmental pattern in a dependent distribution with confluent ground-glass attenuation [3]. These reported H5N1 findings are in strong contrast to the multifocal patches of ground-glass attenuation identified in this patient with novel H1N1.

This fatal case of pandemic S-OIV showed radiologic features suggestive of noncardiogenic lung injury, or ARDS. In ARDS, respiratory epithelial injury with abnormally increased permeability of the capillary endothelium initially produces patchy consolidations on CT and radiography, with evolution to confluent bilateral air-space opacity. The injury to the lung parenchyma may be caused by infection, toxic inhalation, trauma, or emboli and may be caused indirectly by extrapulmonary disease, such as septic shock, pancreatitis, or other metabolic derangement. In our patient, ARDS was associated with a pattern of severe lung injury involving peribronchial inflammation. This patient's CT pattern, however, is also somewhat different from findings generally associated with ARDS. The typical ARDS opacities are predominantly posterior and basal in contrast to the peripheral rounded foci seen in this case, which are also commonly identified in organizing pneumonia–type reactions. In COP, eosinophilic pneumonitis, or hypersensitivity pneumonitis, these ground-glass opacities would be expected to show elements of cellular infiltration, which raises the question on imaging of whether these rounded foci were mainly edema, cellular, or exudative in composition. The autopsy reported evidence of alveolar injury in which the patches of ground-glass opacity paralleled the localized fibrinous and proteinaceous exudates with hemorrhage, macrophages, and reactive pneumocytes. Some notable imaging negatives in this case include the absence of effusions, lymphadenopathy, and lobar consolidations, which are more commonly associated with bacterial, mycobacterial, and fungal pneumonias. Serologic tests did not suggest bacterial coinfection.

Several limitations in this case analysis warrant mention. First, a single case presentation cannot suggest a generalized pattern that can be proven to represent the pathologic mechanism. More cases will certainly need to be analyzed and compared, and we hope to study additional cases in the future. Given the recent emergence of the pandemic virus, it is expedient to present the initial radiographic and CT findings to assist the clinical health care response in the short term, but this research requires further investigation of other radiologic examinations in documented cases. Second, the 5-day time gap between CT and the autopsy limits the accuracy of directly correlating pathologic and radiologic findings. Furthermore, we cannot confirm whether the histologic sections match the anatomic locations of the radiologic pulmonary features on CT, although the multifocality of disease on pathology and radiology suggests that this is not likely a significant factor. Third, the case data presented here encountered some technical imaging limitations, given the severity of the patient's illness, in which CT was performed without IV contrast material (due to progressing acute renal failure) and the radiographs were limited by portable bedside technique in which segments of the chest were not included in some views. Finally, the outcome of this case raises the question of whether it was the inherent virulence of the pathogen, the underlying host vulnerability or host response, or both that contributed to the lethality of this infection, particularly because pathology and radiology both suggest severe alveolar injury. CT and radiography, however, contributed to the early recognition of a noncardiogenic cause with severe progressive disease suggesting air-space infection and inflammation.

In conclusion, this article describes a fatal case of swine-origin influenza A (H1N1) virus (S-OIV) in which CT displayed a pattern of rounded peripheral ground-glass opacities that can be seen with severe peribronchial air-space disease, but were distinguished radiographically from cardiogenic edema. The findings were also suggestive of less airway inflammation than in other reported viral pneumonias. Early CT may help clinicians recognize incipient cases of severe influenza and improve our understanding of the pathogenesis of the disease. Further collection of radiographic data and pathologic–radiologic correlation are warranted.

References

1. Neumann G, Noda T, Kawaoka Y. Emergence and pandemic potential of swine-origin H1N1 influenza virus. Nature 2009;459:931–939. [PubMed: 19525932]
2. Perez-Padilla R, de la Rosa-Zamboni D, Ponce de Leon S, et al. INER Working Group on Influenza. Pneumonia and respiratory failure from swine-origin influenza A (H1N1) in Mexico. N Engl J Med 2009;361:680–689. [PubMed: 19564631]
3. Qureshi NR, Hien TT, Farrar J, Gleeson FV. The radiologic manifestations of H5N1 avian influenza. J Thorac Imaging 2006;21:259–264. [PubMed: 17110849]
4. Ebell MH, White LL, Casault T. A systematic review of the history and physical examination to diagnose influenza. J Am Board Fam Pract 2004;17:1–5. [PubMed: 15014046]
5. Centers for Disease Control and Prevention (CDC). Update: novel influenza A (H1N1) virus infections —worldwide, May 6, 2009. MMWR Morb Mortal Wkly Rep 2009;58:453–458. [PubMed: 19444146]
6. Mollura DJ, Carrino JA, Matuszak DL, et al. Bridging radiology and public health: the emerging field of radiologic public health informatics. J Am Coll Radiol 2008;5:168–173. [PubMed: 18312963]
7. Gunderman RB, Brown BP. Pandemic influenza. Radiology 2007;243:629–632. [PubMed: 17517924]
8. Taubenberger JK, Layne SP. Diagnosis of influenza virus: coming to grips with the molecular era. Mol Diagn 2001;6:291–305. [PubMed: 11774194]
9. Taubenberger JK, Morens DM. The pathology of influenza virus infections. Annu Rev Pathol 2008;3:499–522. [PubMed: 18039138]
10. Hansell DM, Bankier AA, MacMahon H, McLoud TC, Müller NL, Remy J. Fleischner Society: glossary of terms for thoracic imaging. Radiology 2008;246:697–722. [PubMed: 18195376]
11. Remy-Jardin M, Remy J, Giraud F, Wattinne L, Gosselin B. Computed tomography assessment of ground-glass opacity: seminology and significance. J Thorac Imaging 1993;8:249–264. [PubMed: 8246323]
12. Remy-Jardin M, Giraud F, Remy J, et al. Importance of ground-glass attenuation in chronic diffuse infiltrative lung disease: pathologic–CT correlation. Radiology 1993;189:693–698. [PubMed: 8234692]
13. John SD, Ramanathan J, Swischuk LE. Spectrum of clinical and radiographic findings in pediatric mycoplasma pneumonia. RadioGraphics 2001;21:121–131. [PubMed: 11158648]
14. Webb, RW.; Higgins, CB., editors. Thoracic imaging: pulmonary and cardiovascular radiology. Vol. 1st. Philadelphia, PA: Lippincott Williams; 2005.
15. Kim EA, Lee HS, Primack SL, et al. Viral pneumonias in adults: radiologic and pathologic findings. RadioGraphics 2002;22:S137–S149. [PubMed: 12376607]spec no
16. Sullivan CJ, Jordan MC. Diagnosis of viral pneumonia. Semin Respir Infect 1988;3:148–161. [PubMed: 2840725]
17. Layne SP, Monto AS, Taubenberger JK. Pandemic influenza: an inconvenient mutation. Science 2009;323:1560–1561. [PubMed: 19299601]
18. Morens DM, Taubenberger JK, Fauci AS. Predominant role of bacterial pneumonia as a cause of death in pandemic influenza: implications for pandemic influenza preparedness. J Infect Dis 2008;198:962–970. [PubMed: 18710327]
19. Greenberg SB. Viral pneumonia. Infect Dis Clin North Am 1991;5:603–621. [PubMed: 1659594]
20. Mullooly JP, Barker WH, Nolan TF Jr. Risk of acute respiratory disease among pregnant women during influenza A epidemics. Public Health Rep 1986;101:205–211. [PubMed: 3083477]

21. Galloway RW, Miller RS. Lung changes in the recent influenza epidemic. Br J Radiol 1959;32:28–32. [PubMed: 13607979]

22. Tillett HE, Smith JW, Clifford RE. Excess morbidity and mortality associated with influenza in England and Wales. Lancet 1980;1:793–795. [PubMed: 6102679]

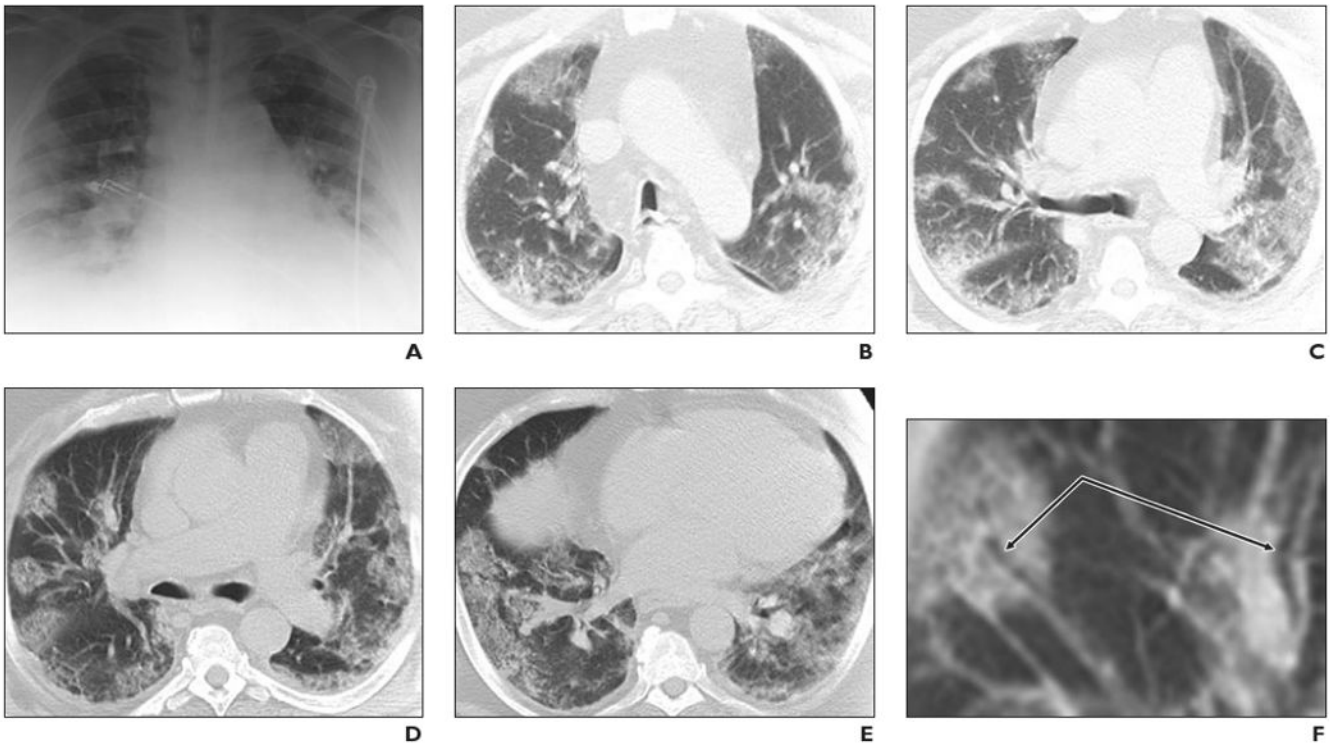

Fig. 1.

Middle-aged man with no history of chronic pulmonary disease presented to emergency department with 5-day history of fever, fatigue, nausea, and diarrhea. He complained of intermittent cough for approximately 3 days and confusion the night before presenting to the hospital. Radiography and CT were performed. Unenhanced chest CT lung window images showed multifocal peripheral ground-glass opacities involving all lobes. Patient died on fifth hospital day.

A, Chest radiograph obtained at clinical presentation shows peripheral opacities.

B, Unenhanced chest CT lung window image shows apical patchy peripheral ground-glass opacities.

C, Unenhanced chest CT lung window image reveals that upper lobe and superior segments of both lower lobes show peripheral peribronchial ground-glass opacities.

D, Unenhanced chest CT lung window image reveals that lingula, right middle lobe, and both lower lobes show patchy, peripheral, rounded, peribronchial ground-glass opacities with air bronchograms.

E, Unenhanced chest CT lung window image shows bilateral lung bases with ground-glass opacities still predominantly patchy at periphery, but more confluent ground-glass attenuation.

F, Magnified view of anterior segment of right upper lobe shows ground-glass opacity peripherally and air bronchograms (*arrows*).